Scanning probe microscopy investigation of gold clusters deposited on atomically flat substrates

2003 J. Phys.: Condens. Matter 15 S2983

(http://iopscience.iop.org/0953-8984/15/42/001)

INSTITUTE OF PHYSICS PUBLISHING JOURNAL OF PHYSICS: CONDENSED MATTER

J. Phys.: Condens. Matter **15** (2003) S2983–S2999 PII: S0953-8984(03)63028-6

Scanning probe microscopy investigation of gold clusters deposited on atomically flat substrates

N Vandamme, E Janssens, F Vanhoutte, P Lievens[1] and C Van Haesendonck

Laboratorium voor Vaste-Stoffysica en Magnetisme, Katholieke Universiteit Leuven, Celestijnenlaan 200 D, B-3001 Leuven, Belgium

E-mail: Peter.Lievens@fys.kuleuven.ac.be

Received 30 April 2003
Published 10 October 2003
Online at stacks.iop.org/JPhysCM/15/S2983

Abstract

We systematically studied the influence of the substrate on the shape, mobility, and stability of deposited gold clusters. The Au_n clusters were produced in a laser vaporization source and deposited with low kinetic energy ($\sim$0.4 eV/atom) on atomically flat substrates (graphite, mica, and gold and silver films on mica) under UHV conditions. Their size distribution is probed with time-of-flight mass spectrometry and ranges from dimers to several hundreds of atoms. Scanning probe microscopy is used to characterize the deposited clusters and the formation of islands by cluster aggregation. On all substrates, Au_n islands can be clearly distinguished and the islands are flattened despite the small impact energy. The shape and size of the island configurations are strongly system dependent. Gold clusters deposited on Au(111) and Ag(111) films grown on mica do not aggregate, but deform due to strong cluster–substrate interactions. The clusters tend to grow epitaxially on these surfaces. On graphite and on mica, deposited clusters do diffuse and aggregate. On the graphite surface, large ramified islands are formed by juxtaposition of small islands and trapping of the clusters at the step edges. On the other hand, the diffusion of the clusters on mica results in a total coalescence of the Au_n clusters into compact islands.

1. Introduction

The growth and study of self-organized nanometre-sized structures is one of the most active fields in recent solid state physics research. Shrinking the size of the devices drastically changes their properties because of quantum confinement effects. The deposition of clusters

[1] Author to whom any correspondence should be addressed.

0953-8984/03/422983+17$30.00

on surfaces is considered a powerful tool for creating nanostructured materials with the desired properties as demanded for technological applications [1, 2]. These small particles not only have specific size- and shape-dependent electronic characteristics, but also their chemical properties, e.g. reactivity and catalytic activity, can be very dependent on the precise geometric arrangement and electronic structure of the supported cluster, in particular for clusters with a diameter smaller than 4 nm. This often results in more selective reactions as compared to the corresponding bulk material [3]. The deposition of clusters, which are pre-formed in the gas phase, offers a large flexibility due to possibilities of carefully controlling the clusters' mean size, kinetic energy, and, eventually, for binary systems, the composition of the deposited clusters [4, 5]. This large flexibility is missing for single-atom deposition by molecular beam epitaxy (MBE) methods, where nanostructures and nanoclusters are grown directly on the substrate through diffusion and aggregation. In that case, the grown structure strongly depends on details of the interaction between the surface atoms and the adatoms, and additional methods need to be implemented to adjust the resulting nanoparticle size distribution [6].

Several parameters determine the final state of supported clusters, such as the cluster size and composition, deposition energy, cluster flux, the amount of deposited material, the substrate temperature, and the kind of substrate. Here, we focus on the influence of the latter parameter, while all other variables are kept unaltered. On varying the surface, the final configuration of the clusters changes from individual clusters through compact structures to large ramified islands. Important here is the difference in lattice mismatch between clusters and substrate material. Previous studies have shown that large antimony clusters on amorphous graphite coagulate completely, while on highly oriented pyrolytic graphite (HOPG) the deposition of these clusters results in a juxtaposition of small islands [7]. For gold clusters, similar differences have been observed [8–10]. On HOPG, high cluster mobility was measured resulting in ramified islands, while on a gold substrate, small compact islands, containing a single cluster or at maximum a few clusters, were detected. In this context only the mobility of clusters as an entity and no perimeter atom diffusion is considered. The term 'island' is used for aggregates of two or more clusters. The aggregation of clusters can either result in a coalescence of the clusters into a compact structure or in a juxtaposition of the clusters or islands.

The final features of the clusters-on-a-surface sample critically depend on the possibility for the clusters to diffuse over the surface: the surface–cluster interactions modify the morphological, electronic, and elastic properties of the deposited clusters or of the formed islands [11]. The behaviour of individual clusters on surfaces can be modelled by techniques based on Monte Carlo (MC) simulations [1, 12], or by means of molecular dynamics (MD) simulations [13, 14]. A combination of experimental results and computer simulations has led to a profound understanding of the growth and the properties of specific cluster-assembled films [15]. In this respect, the investigation of the dependence of the final clusters-on-a-surface structure on both cluster-defined parameters and on the chosen substrate is of fundamental interest.

In this paper we report on investigations of individual low-energy Au_n clusters deposited on atomically flat substrates. The gold nanoparticles are created in a laser vaporization cluster source and their production is characterized by time-of-flight mass spectrometry. The clusters typically have a diameter of 1–3 nm and have a low kinetic energy (typically 0.4 eV/atom) upon impact. As substrate material we used HOPG and cleaved mica, as well as Au(111) and Ag(111) films grown epitaxially on mica. Using scanning probe microscopy (SPM) we investigated the cluster shape and cluster aggregation on the different substrates. The structure of such gold nanoclusters deposited on amorphous carbon and MgO single-crystalline surfaces was investigated earlier with high-resolution transmission electron microscopy [16].

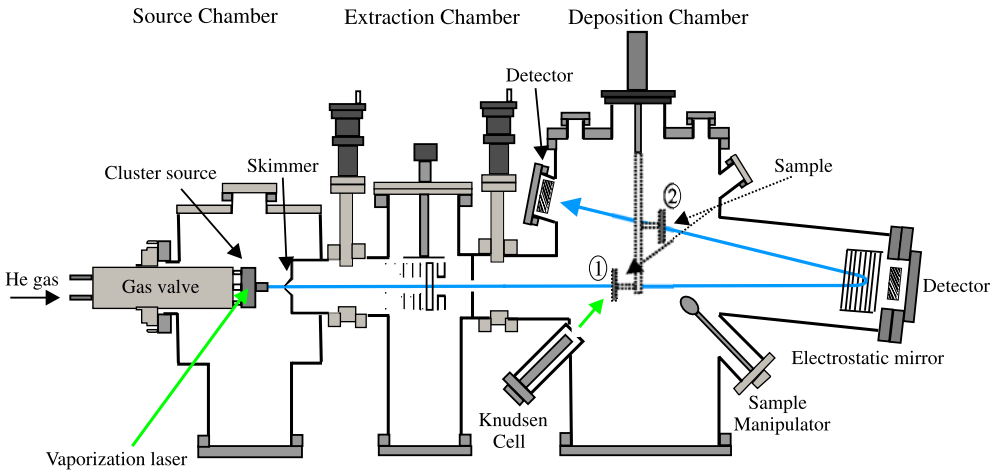

Figure 1. A schematic view of the cluster beam deposition set-up. The apparatus consists of three differentially pumped vessels (source, extraction, and deposition chambers). The set-up is equipped with a dual-target dual-laser vaporization source, extraction optics, a high-temperature effusion cell, a time-of-flight mass spectrometer, and a sample manipulation system. Position 1 (used in this work) and position 2 are two different deposition stages.

(This figure is in colour only in the electronic version)

2. Cluster beam deposition

The Au_n clusters are produced and deposited on the different substrates in a cluster deposition apparatus, schematically presented in figure 1. The set-up consists of three differentially pumped vacuum vessels, named hereafter the source chamber, the extraction chamber, and the deposition chamber. The first two are separated by a skimmer (diameter 2 mm), while the gas flow between the extraction and the deposition chamber is limited by a larger diaphragm (diameter 10 or 20 mm). The source chamber is pumped by a 3200 l s^{-1} (for He) turbomolecular pump (Pfeiffer, TPU 2200) resulting in a base pressure of 10^{-8} hPa. The extraction chamber is equipped with a 1320 l s^{-1} (for He) turbomolecular pump (Pfeiffer, TMU 1600 C) providing a base pressure of 10^{-9} hPa. To obtain a pressure of 10^{-10} hPa in the deposition chamber, a noble gas stable ion pump (Varian, Vac Ion Plus 500) including a titanium sublimation pump with a pumping speed of 410 l s^{-1} is used. The deposition chamber is pre-pumped through the load-lock by a turbomolecular pump (Pfeiffer, TMU 520). The introduction of helium carrier gas during cluster production results in a typical increase of the pressures to 4×10^{-5}, 4×10^{-7}, and 5×10^{-8} hPa respectively in the three subsequent vacuum vessels.

We use a laser vaporization source to produce clusters [17]. A metal vapour is created by pulsed laser ablation (5 ns pulses of Nd:YAG lasers, Spectra Physics, INDI) of the metal target material (spot size of 1 mm^2). The vaporized material is entrained in a short pulse (125 μs) of high-purity cold helium gas (purity 99.9999%), introduced in the cluster formation chamber synchronously with the laser pulse by a pulsed supersonic valve (R M Jordan Company). The metal vapour is cooled by this gas, becomes supersaturated, and condenses in the form of clusters. The targets have a rectangular shape (15×25 mm^2); for the production of bimetallic clusters two rectangular metal targets (7.5×25 mm^2) are used in a dual-target dual-laser configuration. The target is mounted in a brass holder, which is pressed against a slit in the cylindrical formation chamber (diameter 3 mm, length 18 mm). A Teflon seal prevents gas

leaks. Hole drilling in the target by the vaporization lasers is avoided by moving the target holder in a rectangular closed-loop pattern. Two independent laser beams, whose firing time, spot size, and laser energy can be controlled separately, are aligned through two different laser channels in the source. A nozzle terminates the formation chamber. It is possible to alter the effective source geometry by using different nozzles and extension parts of the source. In this study we use a 1.2 mm diameter nozzle with an opening angle of 10°. The timing of the production cycle is controlled by precise delay generators (Stanford Research Systems, DG535) and repeated with a frequency of 10 Hz.

The set-up is equipped with a reflectron time-of-flight mass spectrometer (R M Jordan Company, RTOF). Charged clusters produced directly in the source, or neutral clusters post-ionized by laser photons (e.g. from an ArF excimer laser, Lambda Physik Compex 102, $h\nu = 6.42$ eV) are accelerated electrostatically and mass analysed. For the acceleration we use home-built extraction optics consisting of three grids. The first two are 20 mm apart and are at respectively 3700 and 3400 V. A grounded third plate is located 10 mm downstream. The first two extraction grids are pulsed from ground to high voltage for 500 μs using two fast switches (Behlke Electronics, GHTS 60). Mass-separated clusters are detected with dual microchannel plates. The mass spectrometer has a resolution of about $M/\Delta M = 1000$ around $M = 200$ amu.

The deposition chamber is also equipped with a high-temperature effusion cell (EPI, 10 cm^3), which allows one to grow atomically flat films *in situ*. If clusters are deposited on these substrates, there will be no contamination between clusters and substrate. Furthermore, it is possible to produce films of clusters embedded in an insulating or conducting matrix material.

With the transfer system, multiple samples can be stored in the deposition chamber through a load-lock without breaking the vacuum; a sample manipulator transfers the sample to the appropriate position. Position 1 (see figure 1) is used for the deposition of low-energy particles (kinetic energy of 0.4 eV/atom). This kinetic energy is small when compared to the binding energy of an atom in the cluster, and therefore no fragmentation of the clusters upon impact is expected. For this type of deposition no acceleration voltages are applied, and the extraction optics are moved out of the beam line. Consequently, both charged and neutral clusters are deposited, while an additional electrode in the source chamber allows deflection of the charged clusters. Position 2 (see figure 1) is suitable for the deposition of accelerated cationic clusters that passed the reflectron. In this way, mass-selected depositions are possible with a mass gate (an additional positively biased decelerating electrode) placed in front of the sample, while avoiding destruction upon impact. The sample holder is equipped with a temperature controller, allowing heating up to 900 °C and cooling down to liquid nitrogen temperature.

In this study, clusters were deposited at room temperature on the different surfaces with their inherent low kinetic energy (0.4 eV/atom). By tuning the source parameters, the mean size of the clusters can be set: for this study a value of 15 mJ/pulse was used for the vaporization laser fluence, and the He gas pressure was set at 9 bar. Other source parameters are as described above. A typical cluster abundance spectrum is shown in figure 2(a). The clusters contain up to around 500 atoms. The abundance maximum of the cluster size distribution corresponds to a cluster diameter of 2 nm (or about 250 atoms per cluster).

For interpreting the mass spectra, two limitations should be considered. First, because of the limited and size-dependent mass resolution, the higher-mass peaks will be broader, meaning that the cluster abundance for a specific size does not correspond to the peak amplitudes. Figure 2(b) shows the same mass abundance spectrum, but now with the amplitudes obtained by integrating the peaks of figure 2(a) corresponding to a certain mass (only clusters containing 1,

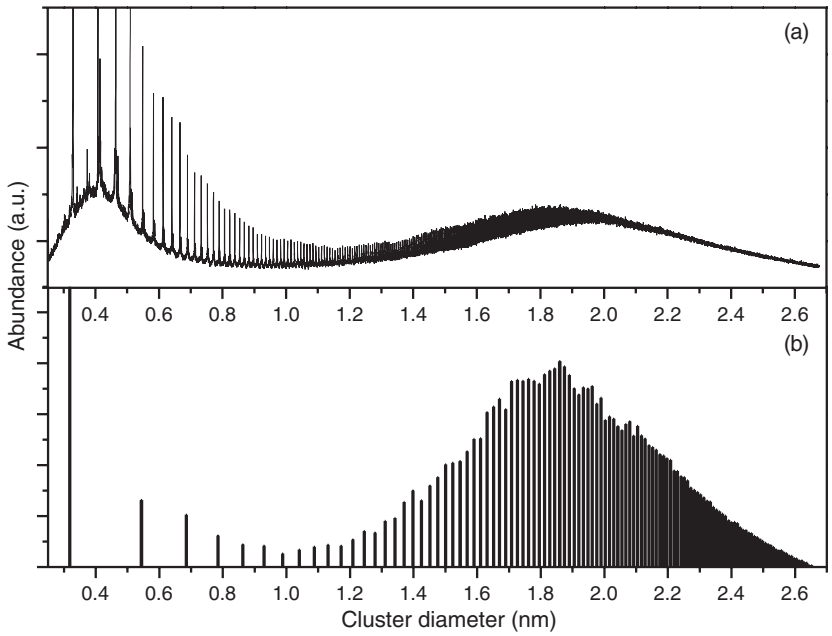

Figure 2. (a) The abundance spectrum as recorded with the mass spectrometer of free cationic Au_n clusters as a function of the cluster diameter. The clusters are assumed to be spherical, with a radius given by $R = r_{Au}\sqrt[3]{n}$, where r_{Au} is the Wigner–Seitz radius (0.159 nm). (b) A histogram of the integrals of the mass peaks corresponding to clusters containing 1, 5, 10, 15, 20, ... atoms. The majority of the clusters have a diameter between 1.5 and 2.2 nm, corresponding to 100–300 atoms, respectively.

5, 10, 15, 20, ... atoms were considered). One can note that the contribution of clusters having a diameter smaller than 1 nm will be negligible in the deposition experiments. Secondly, the ion-to-secondary-electron conversion efficiency of the microchannel plate detector is dependent upon the ion velocity. Heavy ions obtain a lower velocity in the electrostatic acceleration fields leading to a cut-off for higher masses in the mass spectra. This implies that larger clusters may be present in the beam (and on the deposit) while remaining undetected by mass spectrometry.

To study individual clusters, the surface coverage should be well below one monolayer. Deposition times for realizing this coverage typically range between 30 s and 5 min.

3. Atomically flat substrates

A scanning probe study of individual, non-interacting deposited clusters requires a careful choice of substrates. First of all, the substrate must be locally atomically flat to allow one to distinguish the nanometre-sized clusters. Secondly, the mobility of the clusters on the substrate should be limited to avoid cluster aggregation [18–20]. We considered two commercially available flat surfaces, i.e. cleaved HOPG and green muscovite mica, and two home-made systems, i.e. atomically flat Au(111) and Ag(111) films epitaxially grown on mica. The preparation of the latter ones is described in detail below.

A technique commonly used to realize atomically flat gold and silver films is the atomic deposition of a layer on mica with a thickness of a few hundred nanometres [21]. As regards

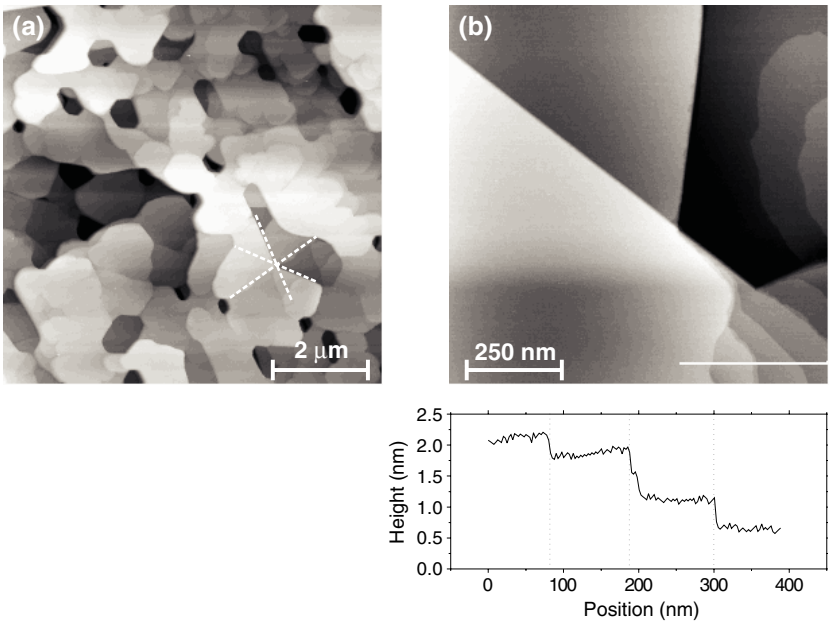

Figure 3. STM images (1 nA, 100 mV) of the Au(111) surface morphology. (a) An $8 \times 8\ \mu m^2$ (the z-range is 50 nm) image illustrating the Volmer–Weber island growth for a gold film grown epitaxially on mica. The three symmetry directions are indicated by the dotted lines. (b) A $1 \times 1\ \mu m^2$ (the z-range is 8 nm) image of atomically flat terraces separated by steps several monolayers in height. In the height profile along the solid curve, the atomic steps have been indicated by the dotted lines. The average roughness R_{ave} on a terrace is 0.06 nm.

specific growth conditions, the (111) plane of gold or silver grows parallel to the (001) plane of the mica [22]. Elaborated studies have shown that the evaporation rate, substrate temperature during deposition, layer thickness, and post-annealing temperature are of great importance for realizing epitaxy between mica and gold [23–31] and mica and silver [32]. Large micron-sized atomically flat areas are obtained for optimized growth parameters. The cleaved green muscovite mica is introduced in a high-vacuum transfer system ($\sim 10^{-8}$ hPa) and degassed by annealing for 1 h at $T = 550\,^{\circ}$C. The films are grown in a MBE chamber with base pressure during deposition of $\sim 10^{-10}$ hPa. The Au and Ag films are deposited by thermal evaporation of high-purity (99.999%) gold and silver. The evaporation rates are calibrated by quartz crystal oscillators and typically range between 0.03 and 0.1 nm s^{-1}. The substrate temperature is controlled resistively and measured with a thermocouple. Although the bulk crystallographic structures of gold (fcc, $a_0 = 0.408$ nm) and silver (fcc, $a_0 = 0.409$ nm) are very similar, the optimum temperature during both evaporation and post-annealing, as well as the optimal film thickness, differ significantly. Hence, we discuss the growth procedure for the two films separately.

Au films with large atomically flat terraces are obtained if the substrate is kept at a temperature of 500 °C during evaporation and at 530 °C during post-annealing for 1 h. At lower evaporation temperatures the number of flat areas decreases drastically, while at higher evaporation temperatures the mica starts to degrade. The minimum film thickness for continuous Au films is 100 nm. Thinner films consist of individual islands, separated by grooves down to the mica, resulting in an electrically insulating film. The as-grown Au films consist of a Volmer–Weber island structure on the micrometre scale, and atomically

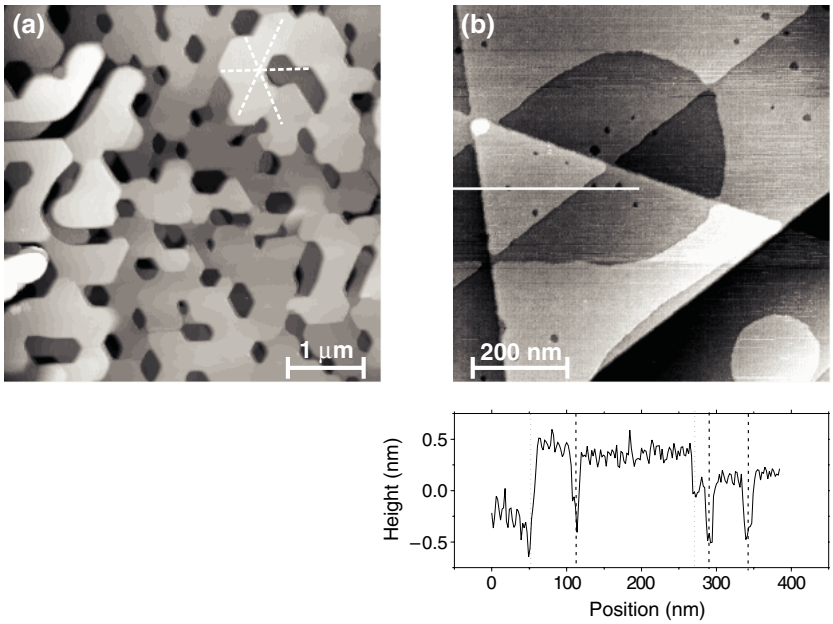

Figure 4. STM images (1 nA, 100 mV) of the Ag(111) surface morphology. (a) A 5×5 μm^2 (the z-range is 80 nm) image where the epitaxy becomes obvious in the hexagonally shaped islands (the symmetry directions are indicated by the dotted lines). (b) An 800×800 nm^2 (the z-range is 4 nm) image of atomically flat terraces on top of a silver island. Monolayer-high steps (indicated by the dotted lines in the height profile) along the three symmetry directions, as well as some holes (indicated by the dashed lines in the height profile) are typical of the silver film morphology. The average roughness R_{ave} on a terrace is 0.1 nm.

flat terraces without any steps having dimensions up to 500×500 nm^2 (figure 3) [22]. The terraces are separated by steps with a height of one or more monolayers ($d_{111} = 0.235$ nm for gold), reflecting the epitaxy (see the cross-section). The quality of the films can be evaluated by calculating the average roughness [28, 29]. R_{ave} typically ranges between 0.5 and 1 nm on the micrometre scale, and between 0.05 and 0.2 nm on an atomically flat terrace. For polycrystalline films, R_{ave} is typically an order of magnitude larger.

The optimal substrate temperature for growing continuous, atomically flat, epitaxial silver films on mica is drastically lower than that for gold. The substrate is held at 230 °C during the evaporation of silver and at 200 °C during post-annealing for 1 h. These lower temperatures result in smaller islands, but for higher temperatures the quality of the films decreases significantly due to the manifestation of numerous defects (e.g. holes one monolayer deep) in the flat areas. At growth temperatures of 230 °C defects are already present, but at this temperature their concentration is low enough not to disturb the analysis of the individual clusters. The percolation limit is reached for 200 nm thick silver films. The morphology of the Ag films is comparable to the Au film morphology, except for the presence of the one-monolayer-deep holes ($d_{111} = 0.236$ nm for silver) on the atomically flat terraces (figure 4). The epitaxy between the mica (001) direction and the silver (111) layer is very pronounced. On the micrometre scale (figure 4(a)) the film consists of islands with hexagonal symmetry. On the nanometre scale (figure 4(b)) steps along the three symmetry directions with heights of 0.236 nm corresponding to one monolayer of Ag(111) are measured.

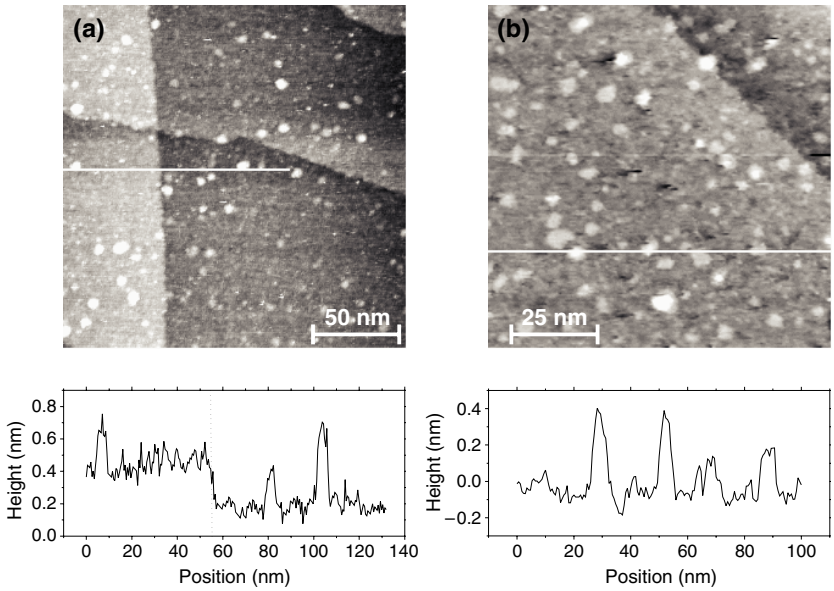

Figure 5. STM images (1 nA, 100 mV) of Au_n clusters deposited on a Au(111) substrate. (a) A 200×200 nm^2 (the z-range is 2 nm) image where the structure of the Au(111) substrate is still clearly visible. No preferential growth of the clusters at the step edges (indicated by the dotted line in the height profile) is observed, and the spreading of the particles is random. (b) A 100×100 nm^2 (the z-range is 1.5 nm) zoomed-in image of an atomically flat terrace. Compact cluster structures are observed, corresponding in size to one individual cluster or an assembly of at most a few clusters.

4. Gold clusters on surfaces

Gold clusters were deposited on the four different substrates, i.e., atomically flat gold and silver films, mica, and HOPG in order to study the influence of the lattice structure on the diffusion, aggregation, and flattening upon impact of the clusters. *Ex situ* ambient atomic force microscopy (AFM) was used to characterize the clusters deposited on mica, and *ex situ* ambient scanning tunnelling microscopy (STM) on the conductive substrates. STM measurements were performed with a commercial instrument (Digital Instruments, Nanoscope II), using Pt/Ir (10% Ir) tips cut with scissors. All STM images were acquired in constant-current mode. AFM measurements were performed with commercial microscopes. Non-contact AFM images were recorded with an M5 microscope from Park Scientific Instruments using silicon cantilevers with a force constant of 2.8 N m^{-1} (Park Scientific Instruments, Ultralevers) and tapping mode measurements were done with a Nanoscope III microscope (Digital Instruments) using silicon cantilevers with a force constant of 40 N m^{-1} (Park Scientific Instruments, Ultralevers).

4.1. Clusters on atomically flat gold films

In figure 5 two STM images of Au_n clusters deposited on a Au(111) substrate are given. The structure of the underlying gold substrate is clearly observable in figure 5(a). A random distribution of isolated particles is present on the flat areas and no enhanced concentration of the clusters is recorded at the steps on the Au(111) surface. Figure 5(b) zooms in on an atomically flat terrace, revealing that the particles are compact and nearly circular. That clusters appear rounded is most likely attributable to perimeter atom diffusion. However, due to resolution

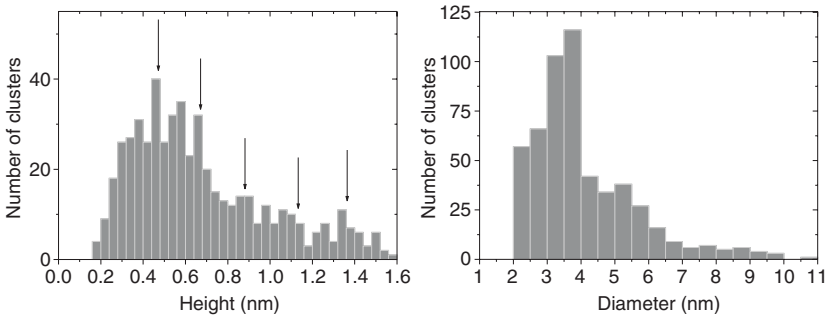

Figure 6. Size histograms of the Au_n clusters deposited on a Au(111) substrate. The arrows in the height histogram indicate the higher abundance for clusters with a height corresponding to a multiple of the Au(111) monolayer thickness (0.235 nm).

limitations at ambient conditions, no conclusions can be drawn on this subject. Typical particle diameters are 5 nm while the typical particle heights are an order of magnitude smaller, as can be seen in the cross-sections given for both STM images.

Using the grain analysis function of a commercially available image analysis software package (Scanning Probe Image Processor (SPIP), Image Metrology) [31], the heights and diameters of numerous particles were determined. All size determinations were done on areas without any steps, to exclude any influence of the substrate morphology. The results are presented in the histograms of figure 6. The typical particle height varies between 0.25 and 1.5 nm, while diameters range from 2 to 10 nm. Taking into account tip convolution effects, the effective island diameter ranges from 0.5 to 8 nm. Relying on the corrected particle size, the volume of the islands was calculated. Most of the particles consist of about 50–1000 atoms. This corresponds to the characteristic size of one single or at most a few deposited gold clusters. Aggregation of the incident clusters on the surface remains very limited for this low coverage, indicating that the clusters do not undergo a significant surface diffusion on the timescale of the experiment.

Comparison of the cluster heights and diameters reveals a large discrepancy between the values: the typical diameters are an order of magnitude larger than the typical heights. First of all, tip convolution effects lead to an overestimation of the determined diameter. Nevertheless, tip effects alone cannot explain this large difference, implying that flattening of the clusters is present. The origin of the strong cluster deformation is twofold. First, the kinetic energy of the impinging clusters causes the clusters to deform upon impact. Second, the perfect match between the cluster and the substrate lattice forces the clusters to grow epitaxially on the surface and partially wet the surface, inducing a flattening of the deposited clusters. The epitaxy is confirmed by the larger abundance of clusters with heights that are a multiple of the Au(111) monolayer thickness (indicated by arrows in the height histogram). These observations are in accordance with previous experiments of gold clusters on Au(111) performed by Bardotti *et al* [8, 9]. In general, small diffusion coefficients are found in case of an epitaxial relationship between cluster and substrate [32].

4.2. Clusters on atomically flat silver films

In figure 7 three STM images of gold clusters deposited on a Ag(111) substrate are shown. Apart from the morphology of the silver film itself (which contains one-monolayer-deep hole-like defects, as discussed above), the topography is very similar to that in the case of the

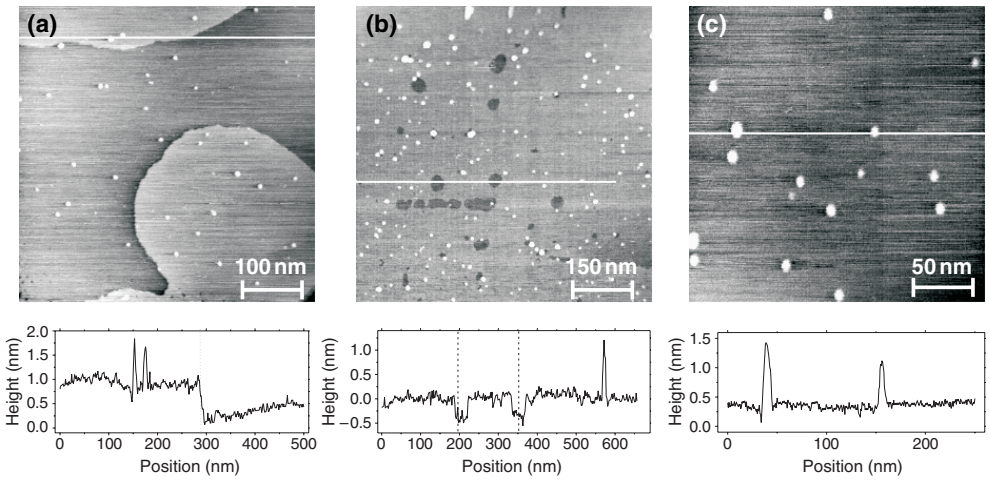

Figure 7. STM images (1 nA, 100 mV) of Au_n clusters deposited on a Ag(111) substrate. The scan ranges are (a) 200×200 nm^2 (z-range is 2 nm), (b) 750×750 nm^2 (z-range is 2 nm), and (c) 250×250 nm^2 (z-range is 1.5 nm). Neither at the step edges in (a) (indicated by the dotted line in the height profile), nor at the defects in (b) (indicated by the dashed lines in the height profile) are higher cluster concentrations observed. (c) The particles measured on top of an atomically flat terrace correspond to single clusters or to aggregates of a few clusters.

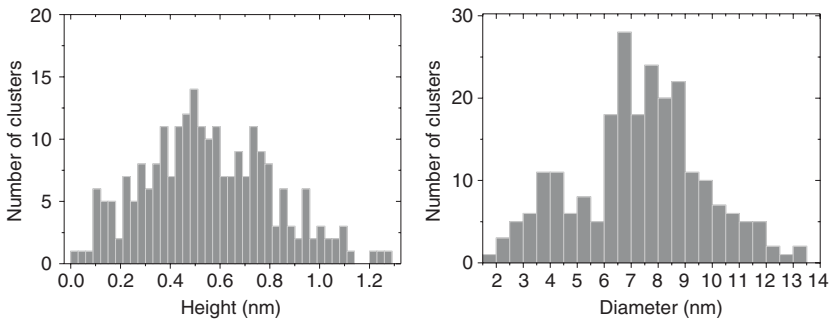

Figure 8. Size histograms for Au_n clusters on a Ag(111) substrate.

Au(111) substrate. On the Ag(111) surface there is no preferential positioning of the particles at the surface steps (see figure 7(a)), nor at the defects in the silver film (figure 7(b)). The clusters are randomly distributed across the substrate. Also here the cluster diameter and height are determined with the SPIP image analysis software, and the results are presented in the histograms of figure 8. Both histograms are very similar to the histograms for clusters on the gold substrates. Small differences between the two systems can be related to the difference in sharpness of the tips used. After deposition, the clusters remain individual; at most a few clusters aggregate. A deformation of the clusters takes place due to impact and interaction with the substrate. Again, the limited cluster diffusion is due to the correspondence between lattice parameters, the mismatch between the gold clusters and the silver substrate being only 0.4%.

The main difference between cluster deposition on a gold and on a silver substrate appears when studying the cluster stability over longer periods of time. On a gold surface the cluster configuration remains unaltered during repeated scanning and as a function of time (even after a few months). On the other hand, on the silver substrate the clusters tend to diffuse.

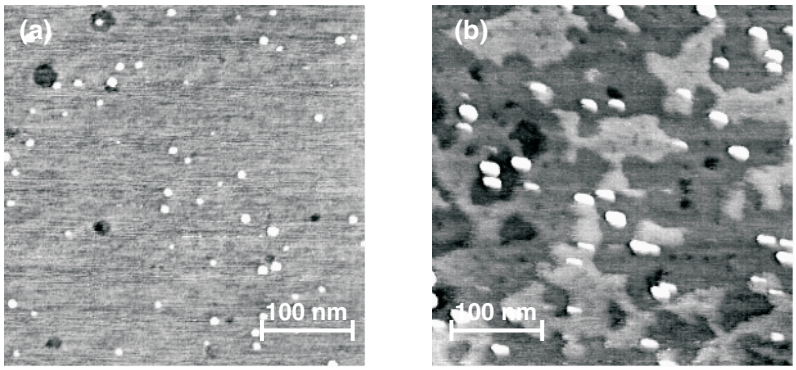

Figure 9. STM images (1 nA, 100 mV, 400 × 400 nm^2; the z-range is 4 nm) of clusters deposited on a Ag(111) substrate. (a) The STM image measured immediately after deposition. (b) The STM image taken after two months. Due to the ageing of the silver substrate, the clusters aggregated into larger islands. The average roughness increases from $R_{ave} \sim 0.15$ nm for the fresh sample (a) to $R_{ave} \sim 0.25$ nm for the aged sample (b).

First of all, silver undergoes a natural oxidation process. When the sample is stored in ambient conditions for longer periods of time (several weeks) the surface starts to age and the atomically flat areas roughen. This gives rise to a rearrangement of the clusters and larger entities are formed (figure 9). On the fresh sample the roughness $R_{ave} \sim 0.15$ nm and the typical particle diameters are 2–12 nm. After two months in air the roughness of this sample has increased to $R_{ave} \sim 0.25$ nm and the typical particle diameters are about twice as large.

A second surface modification process is induced during repeated scanning of the surface [33, 34]. Especially in regions with a lot of defects, scanning changes the cluster configuration significantly. The original hole-like defects tend to form new steps on the silver surface. This is shown in figure 10. In the first scan (figure 10(a)) the clusters are randomly spread. After three scans (figure 10(b)) the holes on the right edge of the STM image start to become larger. This enlargement proceeds and the edges of the defects become straighter (figure 10(c)). Finally, after scanning the same area about ten times, the holes have migrated to form new steps along the symmetry directions of the silver surface (figure 10(d); see the dotted lines). During this step formation, the clusters are forced to diffuse, and coagulate with other clusters and silver atoms. For example, the clusters in the bottom left corner of figure 10(a) have aggregated into new larger islands in figure 10(d).

4.3. Clusters on mica

An AFM image of clusters deposited on a cleaved mica substrate is given in figure 11. Compact island structures spread randomly all over the surface. Since the observation of steps and defects on mica is beyond the AFM resolution for large scan ranges, it is not possible to detect any preferential positioning of the particles at such features. However, given that the particles are distributed randomly on the substrate, the aggregation of the clusters at step edges is improbable. Also, no conclusions can be drawn concerning the preferential nucleation of islands at defects.

Height and diameter determinations of the islands on mica result in the size histograms of figure 12. A first observation is a mean island height of 1.25 nm, differing strongly from the mean particle height on Au(111) and on Ag(111), which was 0.5 nm (see figures 6 and 8). Since the deposition energies and hence the impacts on the surface are comparable in all cases,

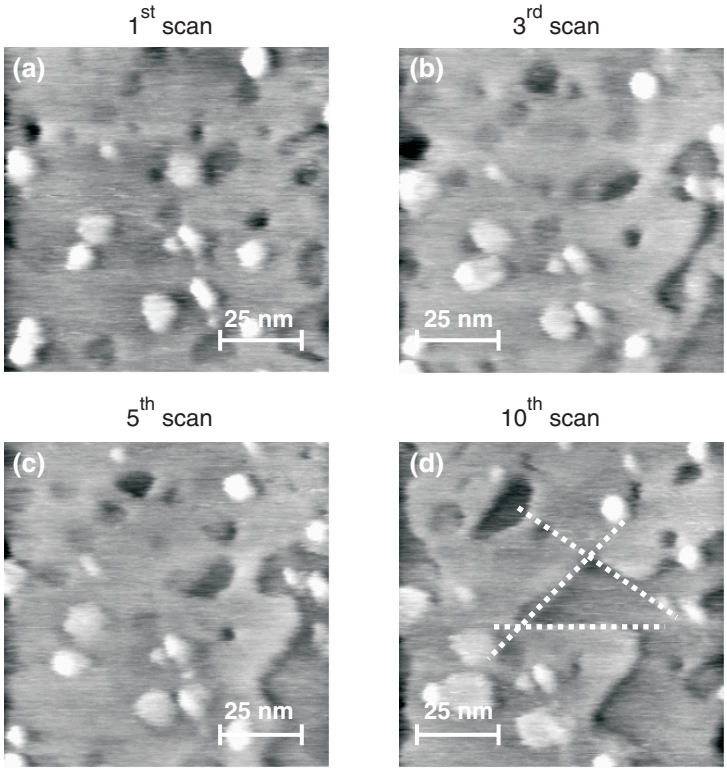

Figure 10. Zoomed-in STM scans (1 nA, 500 mV, 100 × 100 nm^2; the z-range is 5 nm) for the images shown in figure 9. For the first scan (a), the hole and the cluster positions are random. During scanning the holes start to deform (b), resulting in steps (c). After scanning the same area about ten times, the original holes have changed into steps with edges along the symmetry directions (indicated by the dotted lines) of the Ag(111) (d).

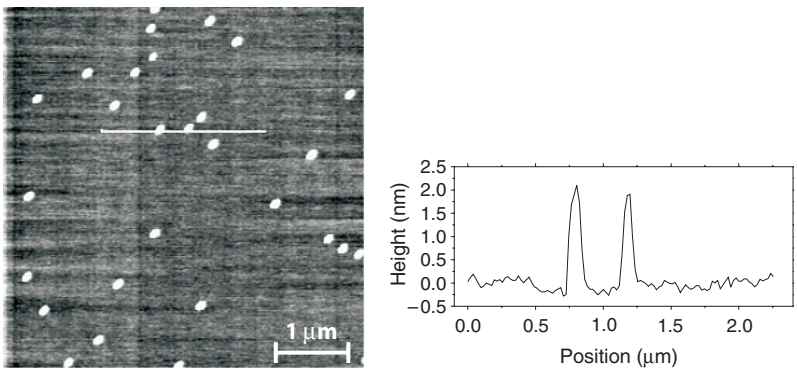

Figure 11. A 5 × 5 μm^2 (the z-range is 4 nm) non-contact AFM image of Au$_n$ clusters deposited on a mica substrate. The diameter and height of the resulting particles do not correspond to the diameter and height of an individual cluster, indicating that coagulation takes place.

the change in mean height can be attributed to the different cluster–surface interaction. As compared to the Ag(111) and Au(111) substrates, the interaction of the Au$_n$ clusters with the

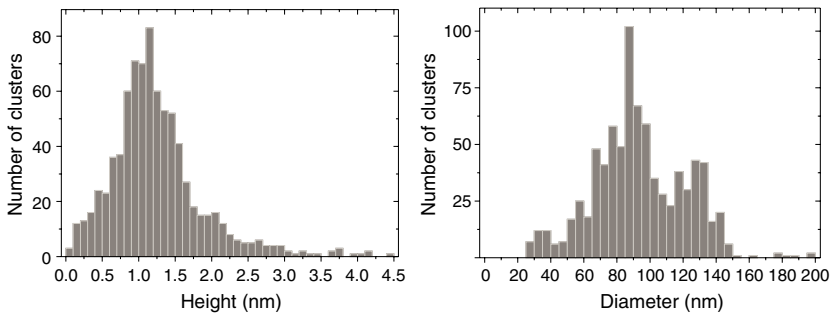

Figure 12. Size histograms of the Au_n clusters deposited on mica.

mica substrate is weaker. This may be attributed to a lattice mismatch of 10% which removes the tendency of epitaxial growth. The cleavage plane of mica consists of a hexagonal structure with lattice parameter 0.520 nm (versus 0.408 nm for fcc gold).

Typical cluster diameters of 40–140 nm are observed for deposition on mica. These large values are not compatible with the dimensions of a single cluster, even when a tip convolution effect (which accounts for a few nanometres at most) is taken into account. The gold clusters must have diffused on the mica substrate and aggregated into larger entities. Again, the cluster–surface interaction may explain the differences from the deposition experiments on gold and silver substrates. Due to the difference in lattice parameters between the mica and the gold clusters, the clusters only feel a weak interaction with the substrate, implying that they remain sufficiently mobile and are able to diffuse and coagulate into islands with other clusters. Since the mismatch is not too large, the cluster mobility remains limited. An island has time to rearrange itself in between two collisions, coagulate, and form a compact structure. One usually assumes that the coalescence process will be stopped as soon as a sufficiently large cluster aggregate has been formed [1, 6]. Indeed, a cluster will prefer to aggregate with another cluster (with high curvature), rather than with a larger island (with low curvature). The critical size, i.e. the size up to which clusters coagulate, is then determined by the time that it takes for a new cluster to arrive. It should be mentioned that during this coagulation process, individual perimeter atoms can diffuse. However, timescales for atom diffusion are much longer, such that the changes in the actual cluster morphology will be small and beyond the AFM resolution under ambient conditions. Considering that the mean island height and diameter correspond to the critical island size, one can calculate that such an island consists of about 20 000 atoms, i.e., about 100 single Au_n clusters.

Because of the specific surface morphology of gold on mica, it is possible to simultaneously investigate the deposition of Au_n clusters on mica and on Au(111) during one single experiment. We deposited a 80 nm thick gold film on mica, all the other parameters remaining unaltered. This thickness is just below the percolation limit (see above), implying that areas of bare mica are still present in between the gold islands. However, for these discontinuous Au(111) films, some small gold droplets are formed in the grooves of the gold layer where the bare mica is being exposed. Consequently, the configuration of clusters originating from the same deposition can be compared in one single image for a gold and for a mica substrate. An AFM image together with the corresponding phase image is given in figure 13. From the topography image (figure 13(a)) no conclusions can be drawn about differences in cluster configuration, because the height differences between the mica and the gold surfaces are too large as compared to the particle heights. In the phase image (figure 13(b)) these height variations are filtered out and the arrangement of the particles can be compared. The difference between the configuration

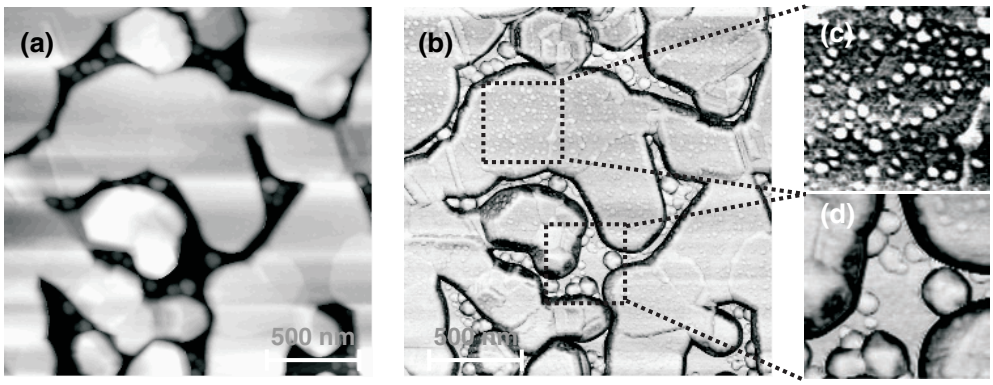

Figure 13. A $2 \times 2\ \mu m^2$ tapping mode AFM image of Au_n clusters deposited on a discontinuous gold film. In the grooves the clusters are deposited on bare mica. (a) Due to the large height differences in the topography (the z-range is 150 nm), no differences can be observed for the cluster configuration on the mica and on the gold. (b) In the phase image (the z-range is 70°), the height difference is filtered and the details of the deposited clusters become clear. On a gold area (c), the particles are randomly spread, while on a mica area (d), the clusters diffused and aggregated with the gold droplets originating from the MBE deposition of the gold film.

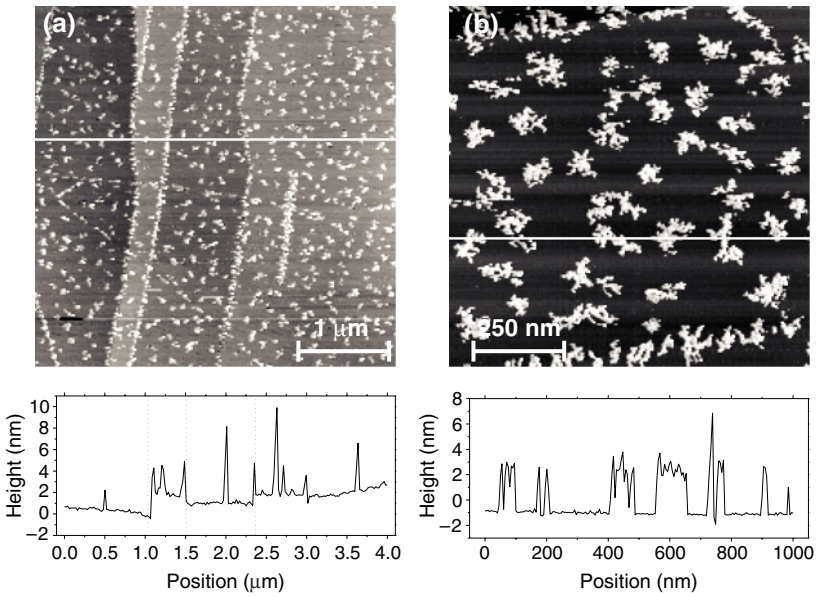

Figure 14. STM images (1 nA, 100 mV) of Au_n clusters deposited on a HOPG substrate. (a) A $4 \times 4\ \mu m^2$ (the z-range is 40 nm) image illustrating the aggregation of clusters at the step edges (indicated in the height profile by the dotted lines). (b) A $1 \times 1\ \mu m^2$ (the z-range is 11 nm) zoomed-in image of the ramified islands on top of a flat terrace. Typical heights of about 3 nm and island diameters up to 100 nm are observed.

on a gold area (figure 13(c)) and that on a mica area (figure 13(c)) is obvious. On the gold area the particles are randomly spread, while an inhomogeneous distribution of larger islands is observed on the mica. The clusters diffused and aggregated with neighbouring clusters as well as with gold droplets originating from the MBE growth process.

4.4. Clusters on highly oriented pyrolytic graphite

Figure 14 shows typical STM images of Au_n clusters deposited on HOPG. Large ramified islands (typical diameters of 100 nm) are found on the flat HOPG terraces. A high island density is observed at the steps (figure 14(a)). Each island is composed of several branches, which are juxtapositions of smaller particles (figure 14(b)). The formation of these large structures, together with the higher island density at the step edges of the graphite where trapping of the clusters takes place, reveals a high mobility of the Au_n clusters on graphite. In contrast to the case for the mica substrate no total coagulation of the constituent clusters takes place. Nevertheless, the clusters on graphite also form compact structures up to a certain critical size; the typical sizes of the smallest branches of the ramified islands are significantly larger than the typical cluster size. If more material is added, no complete coalescence is possible, resulting in fractal-like islands (the high mobility of gold clusters on graphite gives the clusters little time to coalesce—a process that will stop when a third particle arrives). Also, the formation of compact structures is related to substrate-dependent perimeter atom diffusion.

Earlier studies already indicated the high mobility of gold clusters on HOPG [9, 35–38]. Molecular dynamics simulations performed by Deltour *et al* [36] and MC simulations based on the deposition–diffusion–aggregation model [1] reproduced this behaviour. Fractal structures are formed if clusters, in the size range that we use, are deposited on substrates with lattice parameters differing drastically from those of the clusters. If the lattice mismatch between the cluster and the substrate lattice is large, vibrational coupling between these can overcome the small energy barriers of the surface potential. This leads to fast Brownian-like motion of the clusters. Since the graphite surface has a close-packed hexagonal structure with a lattice parameter of 0.246 nm (versus 0.408 nm for fcc gold), the lattice mismatch is 53% and the interaction potential imposed by the graphite surface appears very smooth to the cluster, resulting in high cluster mobility. The small cluster–substrate interaction is also reflected by the height of the particles in the different branches. We measure typical heights of 3 nm, which is about double the mean height value on mica and even six times that on Au(111) and on Ag(111). Given that the cluster–cluster interaction is stronger than the cluster–surface interaction, it can be argued that the clusters reaching the border of an island can mount the growing aggregate [39].

5. Conclusions

SPM was used to indicate the differences in shape, configuration, and stability of Au_n clusters deposited on different substrates. A major influence of lattice mismatch between cluster and substrate on shape and configuration was found. Increasing the lattice mismatch results in a strong decrease of the cluster flattening and an enhancement of the cluster mobility. Surface modifications (tip induced, oxidation) give rise to instabilities of the cluster configuration.

On the graphite surface there is a very large mismatch between the cluster lattice parameters and the lattice parameters of the substrate (mismatch of 53%). The low kinetic impact of the clusters on the surface results in a limited cluster flattening where clusters are able to mount neighbouring particles, and particle heights of 3 nm are measured. The mobility of the clusters is very high, resulting in ramified islands and trapping of the clusters at steps or defects. By artificially creating defects, e.g. nanometre-sized pits, we may obtain an opportunity to create periodic structures of clusters [40, 41].

With a mismatch of 10% for a mica substrate, a larger influence of the cluster–surface interaction is observed. Cluster deformation is present (the mean particle height is 1 nm) and

the low-mobility clusters aggregate into compact islands, consisting of about 100 clusters. These islands may be of great interest as selective binding sites for the attachment of biomolecules [42, 43].

For the study of individual non-interacting clusters, substrates with perfectly matching cluster and substrate lattice parameters are preferable. The strong cluster–surface interaction induces an extreme flattening of the clusters. Typical heights of only 0.5 nm are observed, but the clusters remain separated from each other. In the case of Au_n clusters, both Au(111) and Ag(111) are suitable for achieving such a separation. Moreover, since both substrates are conductive, it should be possible to investigate the electronic level structure in individual clusters as a function of their size using scanning tunnelling spectroscopy [44–49].

The use of Au(111) has two advantages when compared to using Ag(111). First of all, the gold substrate is much more stable. No changes in cluster configuration are observed for periods up to several months or during repeated scanning. A next step in our study of electronic properties of the clusters may be the introduction of a self-assembled monolayer of dithiols in between clusters and the substrate. When the molecules of the monolayer are aligned vertically, a tunnel barrier is created, and single-electron tunnelling effects should be measurable, even at room temperature [50]. The vertical alignment of the dithiols is realized only for deposition on a Au(111) substrate. On Ag(111) the dithiol molecules are oriented horizontally [51].

Acknowledgments

This work was supported by the Fund for Scientific Research—Flanders (FWO) as well as by the Flemish Concerted Action (GOA) and the Belgian Inter-University Attraction Poles (IAP) research programmes. EJ thanks the FWO for additional financial support.

References

[1] Jensen P 1999 *Rev. Mod. Phys.* **71** 1695
[2] Binns C 2001 *Surf. Sci. Rep.* **44** 1
[3] Henry C R 1998 *Surf. Sci. Rep.* **31** 235
[4] Bréchignac C, Cahuzac P, Carlier F, de Frutos M, Masson A, Mory C, Colliex C and Yoon B 1998 *Phys. Rev.* B **57** R2084
[5] Fuchs G, Melinon P, Aires F S, Treilleux M, Cabaud B and Hoareau A 1991 *Phys. Rev.* B **44** 3926
[6] Brune H, Giovannini M, Bromann K and Kern K 1998 *Nature* **394** 451
[7] Bréchignac C, Cahuzac P, Carlier F, de Frutos M, Masson A, Colliex C, Mory C and Yoon B 1997 *Z. Phys.* D **40** 516
[8] Bardotti L, Prével B, Mélinon P, Perez A, Hou Q and Hou M 2000 *Phys. Rev.* B **62** 2835
[9] Bardotti L, Prével B, Treilleux M, Mélinon P and Perez A 2000 *Appl. Surf. Sci.* **164** 52
[10] Bardotti L, Jensen P, Hoareau A, Treilleux M, Cabaud B, Perez A and Aires F C S 1996 *Surf. Sci.* **367** 276
[11] Schaefer D M, Patil A, Andres R P and Reifenberger R 1995 *Phys. Rev.* B **51** 5322
[12] Jensen P, Barabasi A L, Larralde H, Havlin S and Stanley H E 1994 *Phys. Rev.* B **50** 15316
[13] Haberland H, Insepov Z and Moseler M 1995 *Phys. Rev.* B **51** 11061
[14] Hou Q, Hou M, Bardotti L, Prével B, Mélinon P and Perez A 2000 *Phys. Rev.* B **62** 2825
[15] Bréchignac C, Cazuhac P, Carlier F, Colliex C, Leroux J, Masson A, Yoon B and Landman U 2002 *Phys. Rev. Lett.* **88** 196103
[16] Pauwels B, Van Tendeloo G, Zhurkin E, Hou M, Verschoren G, Kuhn L T, Bouwen W and Lievens P 2001 *Phys. Rev.* B **63** 165406
[17] Bouwen W, Thoen P, Vanhoutte F, Bouckaert S, Despa F, Weidele H, Silverans R E and Lievens P 2000 *Rev. Sci. Instrum.* **71** 54
[18] Vandamme N, Verschoren G, Depuydt A, Cannaerts M, Bouwen W, Lievens P, Silverans R E and Van Haesendonck C 2001 *Appl. Phys.* A **72** S177
[19] Carroll S J, Weibel P, von Issendorff B, Kuipers L and Palmer R E 1996 *J. Phys.: Condens. Matter* **8** L617

[20] Radu G, Memmert U, Zhang H, Nicolay G, Reinert F and Hartmann U 2002 *J. Phys. Chem.* B **106** 10301
[21] DeRose J A, Lampner D B, Lindsay S M and Tao N J 1993 *J. Vac. Sci. Technol.* A **11** 776
[22] Reichelt K and Lutz H O 1971 *J. Cryst. Growth* **10** 103
[23] Levlin M, Laakso A, Niemi H E M and Hautojärvi P 1997 *Appl. Surf. Sci.* **115** 31
[24] Liu Z, Brown N M D and McKinley A 1997 *J. Phys.: Condens. Matter* **9** 59
[25] Zheng X Y, Ding Y, Bottomley L A, Allison D P and Warmack R J 1997 *J. Vac. Sci. Technol.* B **13** 132
[26] Putnam A, Blackford B L, Jericho M and Watanabe M O 1989 *Surf. Sci.* **217** 276
[27] Chidsey C E D, Loiacono D N, Sleator T and Nakahara S 1988 *Surf. Sci.* **200** 45
[28] Hegner M, Wagner P and Semenza G 1993 *Surf. Sci.* **291** 39
[29] DeRose J A, Thundat T, Nagahara L A and Lindsay S M 1991 *Surf. Sci.* **256** 102
[30] Baski A A and Fuchs H 1994 *Surf. Sci.* **313** 275
[31] www.imagenet.com
[32] Wen J M, Chang S L, Burnett J W, Evans J W and Thiel P A 1994 *Phys. Rev. Lett.* **73** 2591
[33] Lebreton C and Wang Z Z 1998 *Appl. Phys.* A **66** S777
[34] Li J, Berndt R and Schneider W D 1996 *Phys. Rev. Lett.* **76** 1888
[35] Francis G M, Kuipers L, Cleaver J R A and Palmer R E 1996 *J. Appl. Phys.* **79** 2942
[36] Lewis L J, Jensen P and Barrat J L 1997 *Phys. Rev.* B **56** 2248
[37] Deltour P, Barrat J L and Jensen P 1997 *Phys. Rev. Lett.* **78** 4597
[38] Carroll S J, Palmer R E, Mulheran P A, Hobday S and Smith R 1998 *Appl. Phys.* A **67** 613
[39] Hövel H 2001 *Appl. Phys.* A **72** 295
[40] Siviero F, Barborini E, Boragno C, Buzio R, Gnecco E, Lenardi C, Piseri P, Vinati S, Valbusa U and Milani P 2002 *Surf. Sci.* **513** 381
[41] Bardotti L, Prével B, Jensen P, Treilleux M, Mélinon P, Perez A, Gierak J, Faini G and Mailly D 2002 *Appl. Surf. Sci.* **191** 205
[42] Xiao Y, Patolsky F, Katz E, Hainfield J F and Willner I 2003 *Science* **299** 1877
[43] Maxwell D J, Taylor J R and Nie S M 2002 *J. Am. Chem. Soc.* **124** 9606
[44] Hövel H, Grimm B, Bödecker M, Fieger K and Reihl B 2000 *Surf. Sci.* **463** L603
[45] Tinkham M, Davidovic D, Ralph D C and Black C T 2000 *J. Low Temp. Phys.* **118** 271
[46] Bettac A, Köller L, Rank V and Meiwes-Broer K H 1998 *Surf. Sci.* **402–404** 475
[47] Ralph D C, Black C T and Tinkham M 1995 *Phys. Rev. Lett.* **74** 3241
[48] Li J, Schneider W D, Berndt R and Crampin S 1998 *Phys. Rev. Lett.* **80** 3332
[49] van Bentum P J M, Smokers R T M and van Kempen H 1988 *Phys. Rev. Lett.* **60** 2543
[50] Andres R P, Bein T, Dorogi M, Feng S, Henderson J I, Kubiak C P, Mahoney W, Osifchin R G and Reifenberger R 1996 *Science* **272** 1323
[51] Joo S W, Han S W and Kim K 2001 *J. Colloid Interface Sci.* **240** 391